Predicting effects of E-I balance on the input-output properties of neurons

Alex Reyes

Center for Neural Science, New York University, New York, NY USA

Abstract

In sensory systems, stimuli are represented through the diverse firing responses and receptive fields of neuronal populations. These features emerge from the interaction between excitatory and inhibitory neuron populations within the network. Changes in sensory inputs alter this balance, leading to shifts in firing patterns and the input-output properties of individual neurons and the network. While these phenomena have been studied extensively with experiments and theory, the general operating principles for combining E and I inputs are still unclear. Here, mathematical rules for combining E and I inputs probabilistically are derived that describe how neurons in a feedforward inhibitory circuit respond to stimuli. The model provides insights into the conditions that lead to divisive gain modulation and the generation of various temporal firing patterns, shedding light on the cellular and network mechanisms involved.

Introduction

Features of sensory stimuli are encoded by the activities of populations of neurons in subcortical and cortical areas. After external signals are transduced into action potentials by sensory organs, the resultant activity is propagated through subcortical nuclei, eventually reaching cortex. Much of the stimulus-driven dynamics and receptive field properties of neurons are dependent on the complex interactions between the excitatory (E) and inhibitory (I) neurons at each stage. With changing stimulus, the balance between E and I inputs could shift, resulting in both qualitative and quantitative changes in the sensitivity to inputs and in the evoked firing.

The manner in which neuron responds to stimuli depends on several variables, including the biophysical properties of neurons, the characteristics of the synapses, and network architecture. In reduced, *in vitro* preparation, the activation function or input-output relation (henceforth termed I-O curves) of neurons typically has a step increase in firing rate from zero when the injected current reaches rheobase (minimum current to evoke firing), followed by a monotonic increase in firing rate [1, 2]. The I-O curves *in vivo* are more complex due to network effects. The discontinuous jump in firing near rheobase is often less prominent primarily because background synaptic noise composed of spontaneous E and I from neighboring neurons allow threshold crossing even for weak inputs [3, 4, 5]. With stronger stimuli, the I-O curve can increase monotonically and asymptote to a maximum value or may decrease after reaching a peak [6, 7, 8].

The shape of the I-O curve is not fixed; it can be modulated depending on the animal's state. Stimulus-evoked firing is affected by the state of the animal, e.g. whether it is is at rest or in motion [9] or whether actively attending [10, 11, 12]. In many cases, the tuning acuity is maintained [10,

11]. This phenomenon, known as divisive gain modulation, is thought to result from a change in the slope of the I-O curve without altering the minimum stimulus magnitude required for firing [3, 13]. Experiments *in vitro* suggest that divisive gain modulation is achieved by a combination of synaptic noise and conductance change, both of which act synergistically to produce a change in slope [3]. *In vivo* studies further indicate that local inhibitory neurons play a key role in gain modulation [14, 15]. Finally, simulations and theoretical models propose that gain changes may be mediated by local recurrent connections [16, 17, 13].

In addition to the relative magnitude of E and I inputs, another important variable is the duration and timing of the inputs. Depending on the stimulus, incoming synaptic inputs can brief (5-50 ms), sustained [18, 7, 19, 20]. Because of different time scales activation ranges of voltage gated ion channels, the responses to short and long duration stimuli are likely to differ. In particular, more time is available for integration in longer stimuli. Indeed, gain modulation appears to be different for brief stimuli than for prolonged stimuli. For sustained stimuli, activation of inhibitory interneurons result in divisive gain whereas during brief stimuli, they produced mixed divisive/subtractive effects [14, 15].

Neurons recorded within the same vicinity exhibit a wide range of temporal firing patterns. A sustained stimulus can generate tonic firing that lasts for the duration or phasic responses where the neurons fire only at the onset the stimulus [19, 7, 21, 22] . Moreover, some neurons fire at the onset, the offset, or both ends of the stimulus. Though the responses may be inherited from upstream brain regions [23], some may arise *de novo* via local circuits of excitatory and inhibitory neurons [22, 20] or the biophysical properties of individual neurons [24] .

Understanding the common operating principles that apply across these phenomena would offer significant insights into possible mechanisms. This study aims to derive the mathematical rules for integrating excitatory and inhibitory inputs in feedforward inhibitory circuits. The approach focuses on how these inputs influence the probability of firing and links these changes to the biophysical properties of neurons, as well as the number and strength of excitatory and inhibitory synapses. By doing so, it enables the formulation of an I-O function that aligns with both *in vivo* data and theoretical predictions, while also clarifying the conditions for divisive gain modulation, monotonic vs. non-monotonic I-O curves, and phasic vs. tonic firing.

Results

The circuit examined here is a feedforward inhibitory circuit in which both an E and an I neuron receive excitatory postsynaptic potentials (EPSPs) from an external source, with the I neuron providing inhibitory inputs to the E neuron (Fig. 1A, inset). To explore how E and I interactions influence neuronal firing, the theory is developed in three stages, beginning with idealized networks and advancing to progressively more realistic scenarios.

Estimating effects of E and I on firing probability

To gain insight into basic concepts, consider a highly simplified scenario in which the E cell receives a single excitatory postsynaptic potential (EPSP) from an external source and an equally large inhibitory postsynaptic potential (IPSP) from a local inhibitory interneuron (Fig. 1A). During a stimulus, EPSP and IPSP appear independently with no delay and with equal probabilities p_E and p_I , respectively. Furthermore, the EPSP is sufficiently large to evoke an action potential in the E cell, but can be canceled by the appearance of the IPSP. Although the parameters are identical, the neuron will still fire as long as $p_E \neq 0$ and $p_I \neq 1$. In the example shown Fig. 1A, 4 EPSPs (blue) and 4 IPSPs (red) appear over 7 trials. Only IPSPs that appeared coincidentally with the

EPSP had an effect on firing (trials 3 and 6): trials where IPSPs either failed to appear (trials 1 and 4) or appeared by itself (trials 2 and 7) did not decrease firing. Hence, the firing probability p_F may be expressed as:

$$\begin{aligned} p_f &= p_E - p_E p_I \\ &= p_E(1 - p_I) \end{aligned} \tag{1}$$

where $p_E p_I$ reflects the probability that the EPSPs and IPSPs occur coincidentally.

The surface plot in Fig 1A shows how p_F varies with p_E and p_I and highlights some important properties of eq.1. First, as stated above, the firing probability p_f is non-zero even if p_E and p_I are equal except when p_E =0 and p_I =1. Secondly, p_F depends on how p_E and p_I co-vary. If p_I increases with p_E but at different rates (e.g. $p_I = k_c p_E, 0 \leq k_c \leq 1$), p_F increases monotonically when k_c is close to 0 but non-monotonically when k_c is closer to 1 (orange curves). Third, if p_I is fixed while p_E increases, p_F increases linearly with p_E at different rates (slope = $(1 - p_I)$; green curves). The inset shows the orange and blue curves projected to the p_F - p_E plane. The curves are then effectively the 'input-output' (I-O) relation of the neuron if increases in p_E is interpreted as increases in the stimulus magnitude.

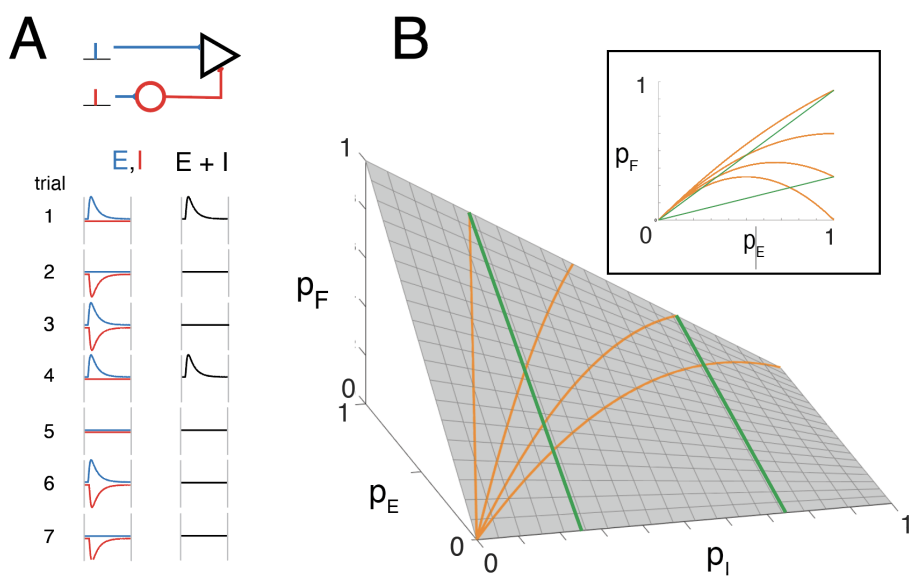

Figure 1: Toy model illustrating basic principles. **A**, top, schematic of a simple feedforward inhibitory circuit. The reference cell (black triangle) and local inhibitory neuron (red) receives a single, suprathreshold afferent input from an external source. Bottom, EPSPs and IPSPs are evoked in the reference cell. The IPSP cancels the EPSP only if it appears simultaneously. **B**, surface plot of firing probability p_f as a function of p_E and p_I . Orange curves show predicted firing probability when p_I co-varies with p_E and green curves when p_I is fixed. Inset, the curves are projected to the $p_F - p_E$ plane

General model

Sensory stimuli can be brief or prolonged, and the cellular events that lead to firing depends on the stimulus duration and so each must be treated separately. Firing evoked with brief stimuli depends primarily on the amplitude and timing of compound excitatory and inhibitory postsynaptic potential. For long duration stimuli, neurons can enter the oscillatory regime where the firing rate depends on the average synaptic current.

Transient firing regime

Stimuli can be brief (5-50 ms) such as tone pips in the auditory system [25, 26, 14] and light flashes in visual system [27]. During these events, each afferent fires a single action potential, resulting in a near-synchronous volley of compound EPSPs, which is then followed, at varying delays, by compound IPSPs from activated I neurons. Whether the postsynaptic cell fires depends on the relative magnitude and timing of the EPSPs and IPSPs. Whole-cell recordings *in vitro* show that IPSPs typically follow EPSPs [28, 29], although in some cases, IPSPs may precede EPSPs [26].

To examine the effects of E -I timing on firing probability, simulations were performed in a network comprised of a single postsynaptic neuron (henceforth termed 'reference neuron', triangle in inset of Fig. 2A). This neuron receives excitatory inputs from a maximum of 100 afferent (actual amount depends on p_E) and inhibitory inputs from a maximum of 100 local I neurons (circles), which are also innervated by the afferents. The arrival times of EPSPs to the reference neuron (and I cells) is Gaussian distributed (Fig. 2A*i,ii*, top panels, blue histograms) and the IPSPs triggered by I neurons occurred after some delay (red histograms). When normalized by the number of trials, the histograms represent the arrival time probabilities of EPSPs and IPSPs, $p_E(t)$ and $p_I(t)$, respectively. The resultant firing of the reference cell occurred well after the onset of the p_E and was more temporally confined (middle panel, gray histogram), indicating a sharpening of the afferent input.

The probability that the postsynaptic cell fires depends on how close the membrane potential is to firing threshold. The time-dependent changes in firing probability can be approximated by convolving the time course of the unitary EPSPs evoked by individual afferent fibers and unitary IPSPs from the I cells with $p_E(t)$ and $p_I(t)$, respectively (see appendix). These probabilities, denoted as $\hat{p}_E(t)$ and $\hat{p}_I(t)$, represent the probability that the membrane potential reaches specific values at a given time. To account for differences in the number and magnitude of inhibition, the inhibitory component is scaled relative to the excitatory component as:

$$p_{net}(t) = \hat{p}_E(t)(1 - k_n k_a \hat{p}_I(t)), 0 \leq k_n k_a \leq 1 \tag{2}$$

where k_n is the ratio of the number of excitatory inputs n_E to the number of inhibitory inputs, and k_a is the ratio of unitary IPSP amplitude to unitary EPSP amplitude. In cortex, $k_n \approx 0.15 - 0.20$ [30, 31] and is set to 0.2 for most of the simulations in this study whereas the EPSP and the IPSP amplitudes are comparable [1, 32, 2] and so k_a is set to 1.

The times of occurrences of the action potentials is computed in two stages. First, the probability $p_\theta(t)$ that the compound PSP exceeds voltage threshold is calculated using a normal cumulative distribution function (eq. 7 of appendix; green curve in bottom trace). Because only single action potential is evoked, the second step is to calculate when the action potential occurs using p_θ and eq. 8 of the appendix. The predicted firing probability (middle traces, magenta) approximates the histogram of evoked spikes. Unlike the toy model, firing cannot be completely eliminated because the IPSP is delayed and so cannot cancel the EPSPs completely. Panel *ii* shows the simulated and predicted responses for a lower intensity stimulus.

The shape of the input-output curves differed from that of the toy model above. In Fig. 2B (top), the magnitude of the inhibitory component was scaled to increase with the input as $p_I = k_c p_E$, with $k_c \in \{0.85, 0.875, 0.9, 0.925, 0.9, 0.975, 1\}$. As k_c increased, the curves deviated from zero at the same point, and although the slope decreased, the curves remained monotonic (Fig. 2B,top). This occurred because the action potentials were generated on the rising edge of $\hat{p}_E(t)$ and near the peak of $p_{net}(t)$, but just when $\hat{p}_I(t)$ was beginning to rise. As a result, there was always a time window in which action potentials could be evoked. When the delay between EPSPs and IPSPs

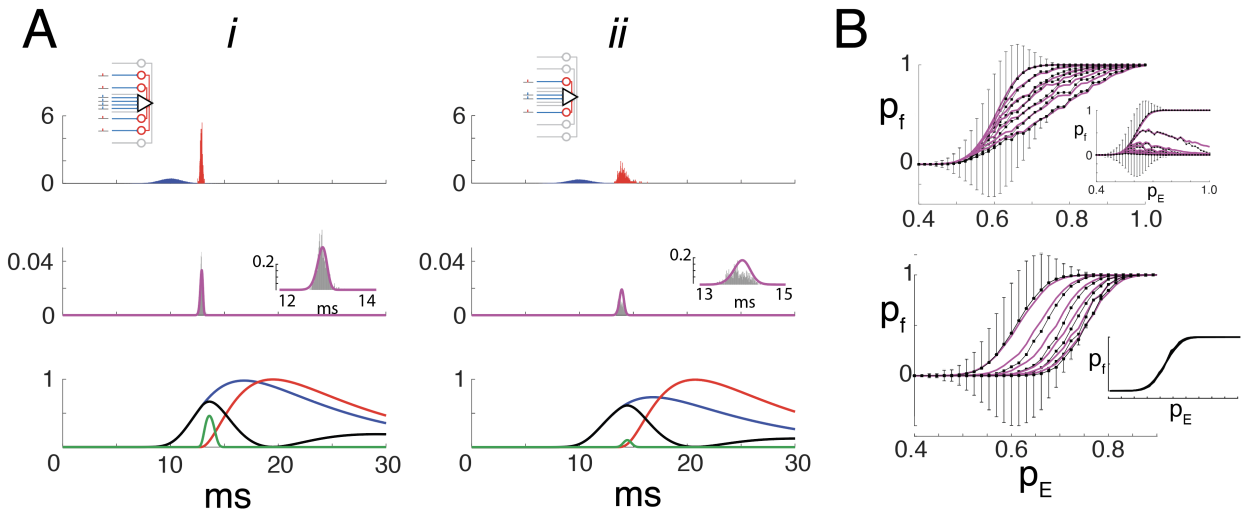

Figure 2: Predicting firing probability for transient stimuli. A*i*,top histograms showing arrival times of EPSPs (blue) and IPSPs (red) in the reference cell. Middle, predicted firing probability (magenta) superimposed on histogram of evoked action potentials in reference cell (gray). Inset, close up of histogram. Bottom, time courses of $\hat{p}_E$ (blue), $\hat{p}_I$ (red), and $\hat{p}_{net}$ (black). The probability that the membrane potential exceeds threshold for firing is shown in green. ***ii*** , same but with weaker input. **B**,top. simulated (black) and predicted (magenta) firing probability as a function of p_E when p_I co-varied with p_E at different rates. Inset, same except the delay between E and I was reduced by 1 ms. Bottom, plot of firing vs p_E with p_I kept at fixed values. Inset, curves are superimposed

was reduced by 1 ms (the inhibitory histograms were shifted by 1 ms to the left), the curves became progressively more non-monotonic with increasing k_c (inset), consistent with Fig. 1B.

In Fig. 2B (bottom), p_I was held constant at specified values ($p_I \in 0.0, 0.4, 0.6, 0.7$) while p_E increased. Unlike the toy model, the curves shifted to the right, indicating an increase in threshold with little or change in the slope (inset). Because p_I was fixed, a higher p_E was needed to increase p_{net} sufficiently to cause threshold crossings. Although the change in p_{net} and PSP amplitude is modest because of the delay, the presence of hard threshold means even small changes in the PSP amplitude will have a significant on firing.

Oscillatory firing regime

For a long duration stimulus, the excitatory afferents and I neurons generate sequences of EPSPs and IPSPs, respectively, producing a synaptic barrage in the postsynaptic, reference neuron. If the input is sufficient large, most cortical neurons transition into an oscillatory firing mode, where the firing rate is determined by the average net synaptic current (i_{net}). Experimentally, the input-output curves are obtained by injecting steady currents intracellularly and then plotting the average firing rate vs current magnitude (aka "frequency-current" or f-I curves) [1, 32, 2].

In Fig.3, simulations were performed where p_E was ramped (ramp duration = 5 ms) to a steady level (*i*, blue trace). Network parameters are as above except the maximum number of E and I inputs ares set to 250 and 50 ($= 0.2 * n_E$), respectively. After a short delay, the I cells fired, resulting in a rapid rise in p_I to the same level (red). The calculated p_{net} (black) has a ramp increase to a peak, followed by a lower steady state level. The firing profile of the reference cell also had a transient increase, followed by a lower steady firing rate corresponding to the onset of p_I (*ii*). The steady state firing depended on magnitude of p_E and p_I : increasing both simultaneously led to a decrease in the steady state level firing (Fig. 3B). While the transient peak corresponded to the period before the appearance of inhibition, it can, as will be shown below, occur even with no delay between p_E and p_I .

To extend the theory to the oscillatory regime, it is necessary to establish the relation between p_E, p_I, and the net synaptic current (i_{net}) generated by the excitatory and inhibitory synaptic barrages. The magnitude of i_{net} is influenced by several factors, including the arrival rate (r_E) and number (n_E) of E inputs from the afferents, the charge generated by each E input (q_E), and the corresponding variables for inhibition. Taking these variables into account, the net current is given by (see eq. 11 in appendix):

$$\begin{aligned} i_{net}(t) &= q_E n_E r_E p_{net}(t) \\ &= q_E n_E r_E p_E(t)(1 - k_n k_q k_r p_I(t)); 0 \leq k_n k_q k_r \leq 1 \end{aligned} \tag{3}$$

where $k_q = \frac{q_I}{q_E}$ is the ratio of the inhibitory and excitatory charges and $k_r = \frac{r_I}{r_E}$ is the ratio of inhibitory firing rate to external excitatory input rate.

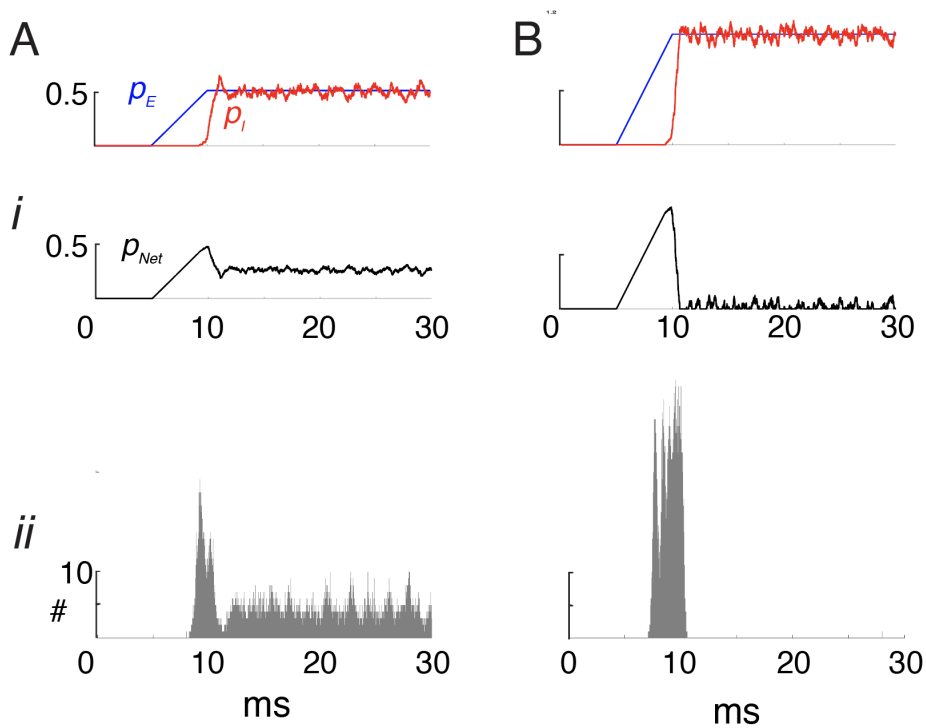

Figure 3: Predicting firing probability for sustained stimuli. **A** *i* top, the excitatory probability p_E (blue) is ramped to a steady value of 0.5. The inhibitory probability p_I (red) develops after a delay of about 5 ms (red). Bottom, calculated p_{net} (black). *ii*, histogram of firing. **B**, same except p_E and p_I was ramped to steady-state values of 1. *Simulation parameters*: The reference neuron and 50 inhibitory neurons received inputs from 250 external afferents, each generating Poisson trains of EPSPs at a mean frequency of $r_E = 50$ Hz. When activated, the I neurons fired ($r_I \approx 20 - 100$ Hz) and evoked inhibitory current barrages in the reference neuron.

To calculate the evoked firing rate r_{osc} in the oscillatory regime, i_{net} is fed to a transformation stage $r_{osc} = S(i_{net})$, where S is an input-output function such as an experimentally measured f-I curve, a model neuron, or in the case of an LIF neuron, the function $1000/(-\tau_m * ln(1 - (i_{rh}/i_{net})))$ with τ_m the membrane time constant and i_{rh} the rheobase current.

Fig. 4A plots firing rate versus p_E when p_I co-varied with p_E at different rates ($p_I = k_c p_E; 0 < k_c \leq 1$). When p_I varied weakly with p_E (low k_c), the evoked firing increased monotonically. As k_c approached 1, the curves flattened and eventually became non-monotonic. The minimum p_E needed to evoke firing (≈ 0.2) was the same for all curves primarily because the E input did not engage the inhibitory neurons until a threshold level p_E was reached. The inset plots the p_E , p_I , and p_{net}

for the most non-monotonic curve (orange). p_{net} deviated from linearity when p_I began to rise, trending downward due to the faster increase in p_I. Fig.4B (*i-iii*) shows the steady-state current for increasing p_E and p_I (top) and associated firing histogram (lower) for points corresponding to the orange curve in A. For modest p_E (i), the net current was above rheobase. As p_E increased (ii), the net current and evoked firing (bottom) decreased and eventually became too small to evoke firing (iii).

When p_I was fixed while p_E increased, the I-O curves changed in two ways: there was a rightward shift in the curves indicating a larger p_E to evoke firing and the slopes became shallower, indicating a decrease in gain (Fig. 5A). Functionally, with this manipulation, gain is both subtractive and divisive (see [13]).

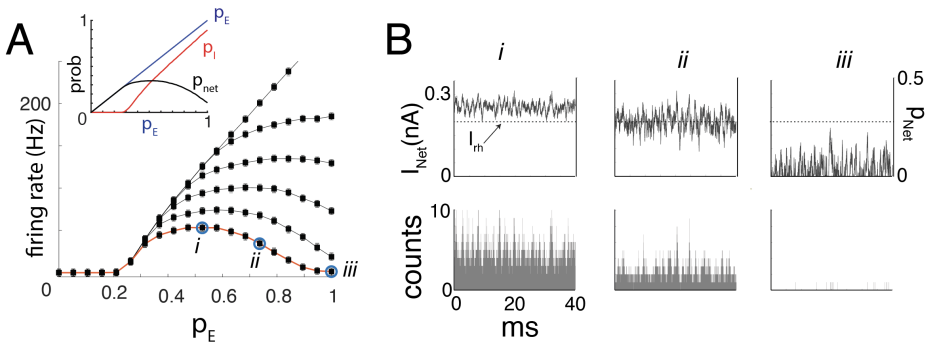

Figure 4: Input-output curves for sustained stimuli when p_I co-varied with p_E .**A**, plot of firing rate vs p_E ; each curve is for different co-variation rates k_c With increasing k_c, the curves switched from being near linear to completely non-monotonic (orange). **B*i-iii***, top, net synaptic current at steady-state for points on the orange curve in **A**.

The input-output curves (Fig.5A) increased smoothly from zero, rather than discontinuously [1, 32, 33], indicating that firing occurred even when the average net current was below rheobase. This is due to inherent fluctuations in the current, which occasionally exceed I_{rh} even when the mean i_{net} is low (Fig. 5B,*i*). The firing rate in this sub-oscillatory range (A, cyan,) can be described by the following expression (see appendix):

$$\begin{aligned} r_{fluct} &= r_{rh}\text{prob}(i_{syn} \geq i_{rh}) \\ &= r_{rh}(1 - \beta(n_E, n_\theta, p_{net})) \end{aligned} \tag{4}$$

where r_{rh} is the minimum firing rate at i_{rh} , β is the cumulative distribution function for a binomial process, and n_θ is the minimum number of excitatory afferents to needed to achieve i_{rh}. The firing rate for the entire range of p_E is then defined to be the larger of r_{fluct} and r_{osc} or $r_f = max(r_{fluct}, r_{osc})$. At high p_E values (B,*ii*), where the average currents exceed or equal i_{rh}, firing transitions into the oscillatory range (r_{osc}, A, green). The equations for r_{fluct} and r_{osc} predicted the decrease in slope and rightward shift in the I-O curves in both the sub-oscillatory and oscillatory regime when p_I was held constant at various levels (C, cyan and green curves).

Spatiotemporal firing profiles

Under physiological conditions, the temporal profile of p_E and p_I depend on several factors including the passive/active properties of the different types of E and I neurons [34] and synaptic delays [26]. In Fig. 3, for example, the delay in the development of p_I partially reflects the membrane time constant and threshold of the I neurons as well as the amplitude and time course of their incoming excitatory inputs. Depending on the identity of the inhibitory neurons or the source of afferents,

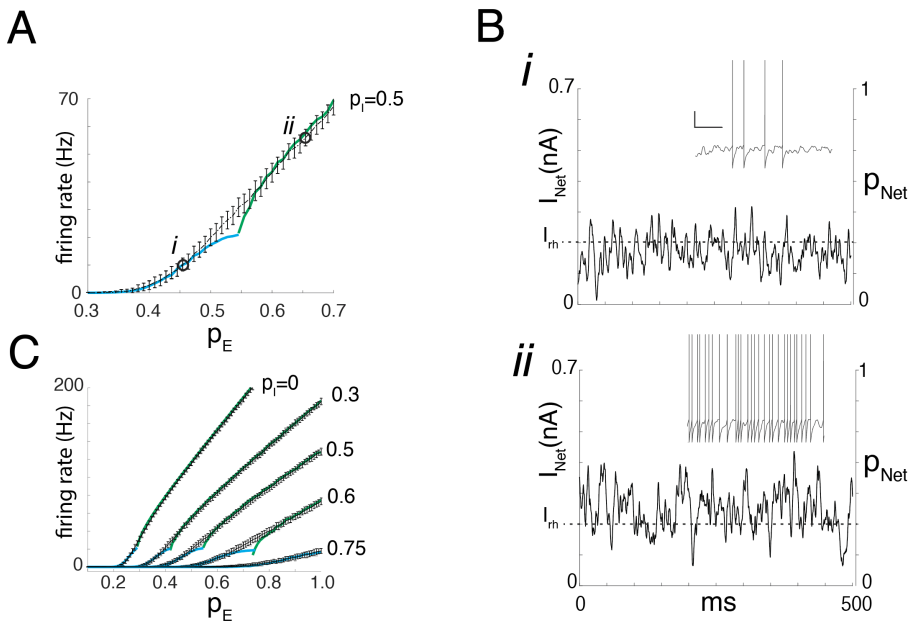

Figure 5: Predicting fluctuation-dominated firing. **A**, I-O curve obtained with p_I fixed at 0.5. Superimposed are the predicted firing at the sub-oscillatory (cyan) and oscillatory range (green). Circled points correspond to traces in B. **B**i, the average net current generated with low p_E is below rheobase (dashed line). Inset, example of evoked firing. scale bars: 10 mV, 100 ms. ***ii***, same but with high p_E . **C**, I-O curves for different fixed value of p_I .

the characteristics of p_E and p_I could therefore vary significantly. To explore the salient effects of different p_E and p_I time courses without having to perform simulations with different cell types, the inhibitory neurons were bypassed and the inhibitory inputs to the reference cell was calculated in manner similar to and independent of the external p_E but obeyed eq. 1.

Many of the temporal firing profiles documented *in vivo* [19, 7, 21] can be reproduced by adjusting the magnitudes of p_E and p_I equally but varying the relative delays. With no delay (Fig. 7B), firing profile was tonic for weak inputs (i) because the p_{net} calculated with eq. 3 was non-zero. When p_E and p_I were increased to near 1, the tonic component decreased and eventually disappeared, leaving the onset and offset responses (ii). Though the p_E and p_I co-varied exactly, the transient responses remained because p_{net} was not zero at the onset and offset (black traces, Aii,bottom). Similar results were obtained when p_I was delayed by 1 ms, except that only the onset firing remained with increasing stimulus (B). When p_I preceded p_E by 1 ms (C), only the firing at the end of the stimulus remained.

In topographically-organized networks, the synaptic drive to a neuron is strongest for a neuron tuned to the stimulus feature and weaker for a neuron further away that is not optimally stimulated. Because the temporal firing profile depends on the magnitude of the stimulus, one prediction is that there will be both qualitative and quantitative differences in the responses of neurons across the network. To examine the spatiotemporal profile of a network, simulations were performed with 80 reference cells in a 1 dimensional network. The p_E of the afferent input is Gaussian distributed (peak = 0.6; $\sigma = 5$ cells) in space (C,left) and lasted 80 ms. The inhibitory input was also Gaussian with the same magnitude but had a wider distribution ($\sigma = 10$ cells). In addition, each reference cell received a background tonic input (p_{back}) that was added to p_E ($p_{E,total} = p_E + p_{back} - p_E p_{back}$) to induce spontaneous firing before the stimulus.

The resulting spatiotemporal profile of p_{net} (B) and the associated firing profile (A) had complex

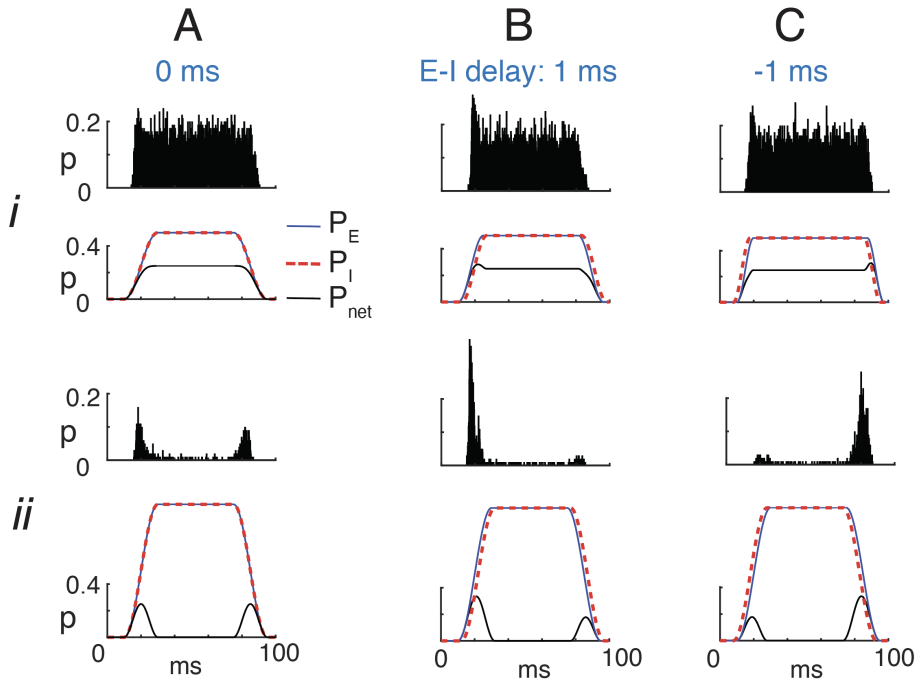

Figure 6: Effects of I delays on spatio-temporal firing. **A**, Simulations were performed with a reference cell that received inputs from a maximum of 250 afferent inputs and 50 inhibitory neurons. p_E and p_I tracked each other with no delay. ***i*** , bottom, when steady-state value of p_E (blue) and p_I (red) were set to 0.5, p_{net} (black) and associated firing (top) were tonic. ***ii***, same except steady-state value of p_E and p_I were set to 1. Neuron fired only at onset and offset of stimulus. **B-C**, same as **A** but with p_I at different delays.

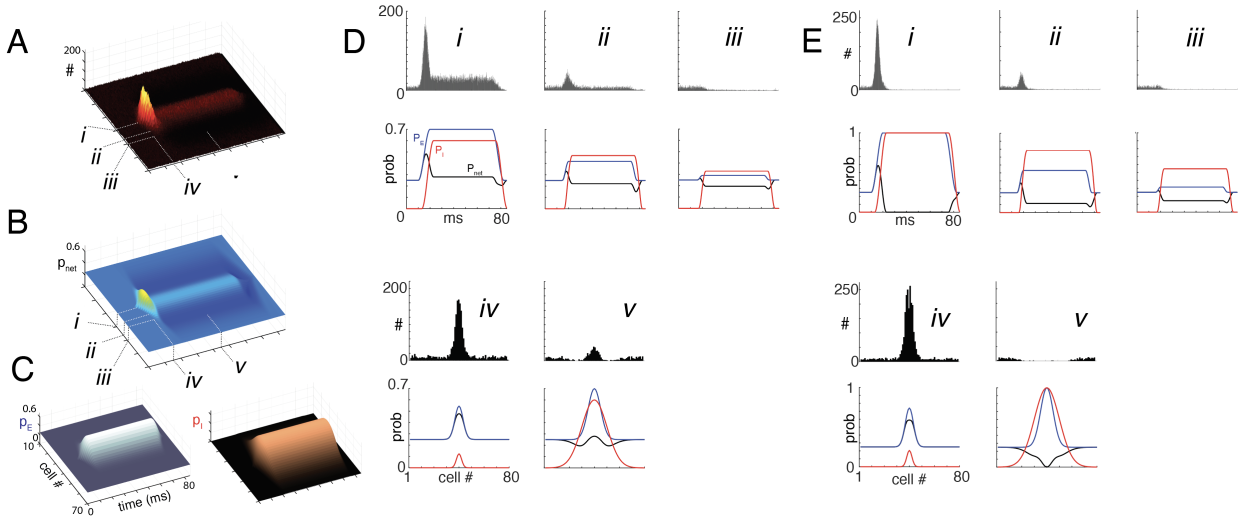

Figure 7: Spatiotemporal firing in networks Simulations was with a 1 dimensional network of 80 reference cell, each receiving a maximum of 250 afferent and 50 inhibitory inputs. Input p_E is Gaussian distributed in space and lasted 80 ms. The p_E and p_I were varied independently. **A**, spatiotemporal activity. **B**, Underlying spatial distribution of p_{net} . **C** , spatiotemporal profile of p_E (left) and p_I (right). **D*i-v*** evoked activity (top) and underlying probability profiles for slices through the spatiotemporal profile labeled i-v in **A** and **B**. **E*i-v*** , same except input p_E was larger.

features. The temporal profile of the neuron at the center had a prominent peak the the onset followed by tonic firing (Fig. 7D*i*). The response of a neuron slightly away from the center (*ii*) had a smaller peak followed by baseline activity, while a neuron further away (*iii*) had only a trough with no peaks. The spatial profile of responses of neurons near the stimulus onset had a prominent peak (*iv*) while that at steady state (*v*) had a peak flanked by troughs. For a stronger stimulus (E, $p_E = p_I = 1$), firing was phasic and the troughs following the peaks reached 0.

Modulation of tuning

Modulation of tuning properties of neurons has been linked to features of the input-output curves [3, 13]. During attention, for example, the response amplitudes change but the relative tuning remained unchanged. When normalized to a peak of 1, the curves before and during attention superimposed [35, 10], indicating divisive rather than subtractive gain modulation, which would broadened the attended curve. Changes in slopes of the input-output curves has been proposed as a mechanism for gain modulation [3, 13]. Therefore, a possible mechanism for modulation is the shifts in the balance between excitation and inhibition with increasing stimulus intensity (Fig. 4A,5A). For these simulations, a tuned input was modeled with a Gaussian curve ($\sigma = 5$ neurons, Fig. 8, middle inset) and then delivered to the network under two conditions. The peak of the tuned input is set to 0.35 to produce firing rates in the 20 to 60 Hz range.

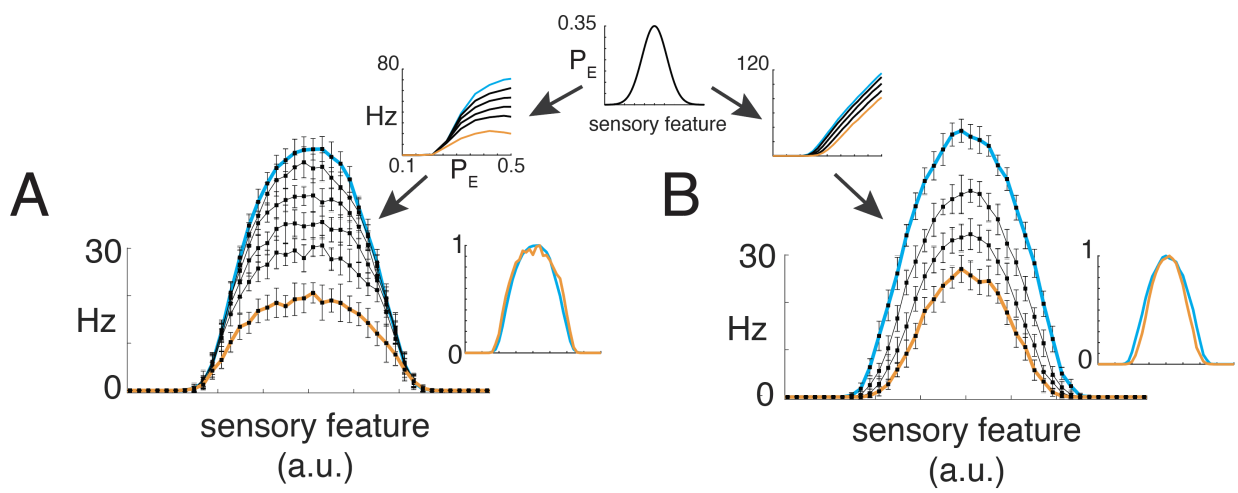

Figure 8: Modulation of tuned receptive fields. Simulation was a reference neuron that received inputs that was Gaussian distributed over an arbitrary tuned feature (middle inset). **A**, response of the reference neuron when p_I co-varied with p_E (I-O curves in right insets). Right inset, the largest (cyan) and smallest (orange) curves were normalized and superimposed. **B**, same except p_I was fixed at increasing values (upper left inset))

One way of achieving divisive gain modulation is by changing the degree to which p_I co-varies with p_E (i.e. $p_I = k_c p_E$; Fig. 4A). Increasing the co-variation constant (k_c) reduced the peak response amplitude (Fig. 8B). The width of the curves for small p_E did not change and the points where the curves deviated from zero are identical. However, as k_c approached 1, the curves became disproportionately broader (lower right inset), reflecting the flattening of the I-O curves (upper right inset).

Another way is to fix p_I at specified values as in Fig. 5C. As observed previously, the curves decreased in amplitude (Fig. 8B). The widths of the curves decreased but the normalized curves superimposed, indicating minimal change in the tuning acuity. This might be unexpected in given the rightward shift in the I-O curves (Fig 5C); however, only small changes in p_I were required

to achieve the targeted firing rates. As shown in the upper left inset, the change in firing rate is considerably larger than the rightward shifts in the curves.

Effects of synaptic conductance

A key assumption in deriving eq. 3 , is that the excitatory and inhibitory inputs sum linearly (see eq. 11 in supplementary material), which is not generally true under physiological conditions since synaptic input will produce conductance changes that can lead to sublinear summation (e.g. shunting inhibition). Thus, the net current calculated at resting potential will be different from that calculated when the neuron is active and the membrane potential is dynamic. .

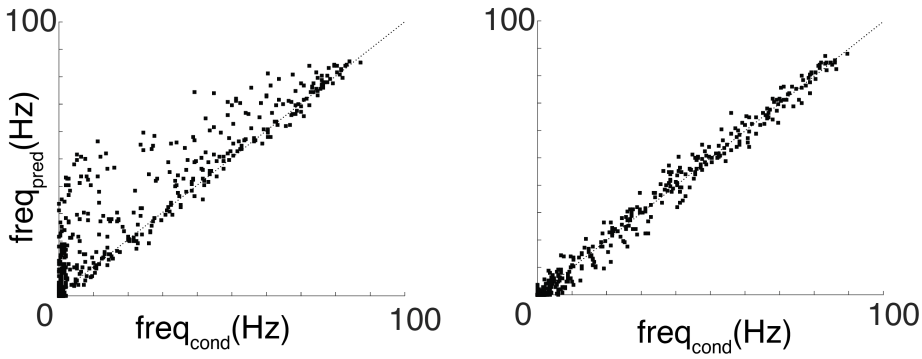

Figure 9: Effects of conductance. **Left**, plot of predicted firing assuming the PSPs summed linearly vs firing rate evoked with conductance-based synapses. **Right**, same but with correction term for voltage-dependent non-linear summation of PSPs.

To examine how non-linear summation affects the predicted firing, simulations were performed as described above, but with synaptic inputs modeled as conductances rather than current. To ensure equal amplitudes ($250\mu V$ for EPSPs, $-250\mu V$ for IPSPs) at resting potential (-70 mV) and with an inhibitory reversal potential of -80 mV, the inhibitory conductance needed to be 7 times larger than the excitatory conductance. The resulting firing rate (f_{cond}) was compared to that predicted (f_{pred}) when the E and I inputs were first combined using eq. 3, assuming linear summation of synaptic currents without voltage dependence, and then delivered to the reference cell as i_{net}. To explore the firing rates under different conditions, the simulations were performed with a random combinations of p_E (ranging from 0.6 to 1), p_I (0.5 to 1), and ratio k_n (0.5 to 1) across 1000 trials. Plotting the frequencies against each other (Fig. 9) (left) shows that f_{pred} overestimated f_{cond}, as many of the points lie above the unitary slope line (dotted).

To correct for the effects of conductance, voltage-dependent terms were added to eq. 3 (see eq. 17 in appendix):

$$\begin{aligned} i_{net} &= q n_E r_E G_E (v - V_{exc}) p_{net} \\ p_{net} &= p_E (1 - k_r k_n k_g k_v(v) p_I) \end{aligned} \tag{5}$$

where G_E is the integral of the excitatory conductance of a single afferent, $k_g = \frac{g_I}{g_E}$ (=7) is the ratio of inhibitory to excitatory conductance, $k_v(v) = -(\frac{v - V_{inh}}{v - V_{exc}})$ with $V_{inh} = -80, V_{exc} = 0$ the reversal potentials for E and I , respectively, and v is the average membrane potential generated by the barrage excluding action potentials. To maintain mathematical rigor, the correction term is valid for $-v_{inh} \leq v \leq v_{inh}/(1 + k_r k_n k_g))$ since probability cannot exceed 1. In practice, however, the inhibitory term can be capped at 1, as the neuron will not fire beyond this threshold. By using this updated equation to generate i_{net}, the match between the two frequencies improved significantly

(Fig.9, right). Thus, with the appropriate correction term, the model is valid for conductance based synapses.

Discussion

The goal of this study is to elucidate the fundamental principles underlying the integration of excitatory (E) and inhibitory (I) inputs in response to stimulus-driven events. Neuronal responses are primarily shaped by the balance between E and I inputs, both of which vary with the stimulus dynamics and strength. By focusing on the probabilities of EPSPs and IPSPs arriving at a neuron, a simple relationship is derived to describe how E and I inputs scale with stimulus magnitude. The results are broadly applicable, as a single model with consistent network parameters can replicate many response features that would have previously required different models.

Relation to previous work

Experimentally, the input-output properties of neurons has been studied by injecting currents, which serve as a surrogate for synaptic activity, and measuring the resulting firing rate. A key observation is a discontinuity near rheobase, by a jump in firing rate followed by a near-linear rise (at least for modest inputs). Most rate models [36, 16, 5] use some form of rectified activation curves (to limit minimum firing rate to zero), some in combination with background noise to remove the discontinuity [5, 4]. By using probability (p_E) as a proxy for input, rectification comes automatically and the noise is inherent and predictable. Importantly, the firing can be directly linked to single cell and network parameters in the equations.

The input-output curves consist of two distinct regions. For small p_E (i.e., weak stimuli), the firing primarily driven by variability in the input, as described by eq. 4. A key factor is a term related to the binomial cumulative distribution function (or equivalently, the normal cumulative distribution function), which results in the hyperbolic-like increase in firing. This smooth, supra-linear increase in firing resembles, to a first approximation, the power-law input-output curves [5, 37], which have been shown to be essential for contrast invariance in the visual system. In some models, this power-law behavior is achieved by synaptic noise into the neuron [37]. In the present model, noise can explicitly calculated from p_{net} .

Changes in the slope of the input-output (I-O) function have long been suggested as a key mechanism for gain control [13]. Gain control, in particular divisive, is essential for maintaining tuning accuity across different cognitive states (e.g., attention [10]) and for limiting responses to high-intensity stimuli (e.g., contrast saturation [5]). In this model, where p_E represents the stimulus magnitude or intensity, the slope of the I-O function can become steeper by decreasing the rate at which inhibition changes with input (e.g. $p_{net} = p_E(1 - k_c p_E)$) (Fig. 4B). Physiologically, altering the parameter k_c could reflect changes in the sensitivity of inhibitory cells to input (i.e. via neuromodulation) and/or an increase in the recruitment of local inhibitory cells with increasing stimulus intensity. These modifications apply to both sub-oscillatory and oscillatory regimes. Moreover, gain can be modulated by varying p_E at different fixed values of p_I (Fig. 5C). Though partially subtractive, the slight shift in the threshold is considerably smaller than to the change in firing rate (Fig. 8). Unlike earlier models of gain modulation, the current model does not rely on recurrent excitatory connections, external noise sources, or conductance changes.

Experiments show that the contribution of inhibition to gain modulation depends on the stimulus duration. Optogenetic activation of parvalbumin-expressing interneurons results in predominantly divisive gain modulation for long duration stimuli [20] but a mixture of divisive and subtractive effects for short duration stimuli [14]. The simulations indicate that gain for brief stimuli is very

sensitive to the relative timing of EPSPs and IPSPs and on on how p_I co-varies with p_E (Fig.2B). Depending on the degree to which optogenetic stimulation overrides the normal physiological drive of PV cells, gain could be divisive if p_I still co-varies with p_E (Fig.2B,top) or subtractive if p_I is effectively constant (bottom). In contrast, gain for long duration stimuli is less sensitive to how p_I co-varies with p_E (Fig. 8) .

The model suggests that the non-monotonic rate-level functions [6, 7, 8, 38] depends on how p_I co-varies with p_E (Fig. 4). This is consistent with experiments [38] and rate models [28], which indicate that imbalanced recruitment of inhibitory inputs is needed for non-monotonicity. In the present model, the non-monotonicity arises when p_I co-varies with p_E at nearly the same rate , causing p_{net} to approach become 0 when p_E and p_I approach 1. In this context, the degree of monotonicity depends on the factors that affect p_I in eqs. 2, 3. These include the sensitivity of I neurons to input (r_I), the relative magnitudes of IPSP and EPSP (k_q), which may be affected by facilitation or depression [2], and the number of recruited I neurons (k_n).

The model reproduced many temporal firing patterns observed in *in vivo* studies [19, 39, 40, 21] by simply adjusting the magnitudes and timing of p_E and p_I (6). For example, increasing stimulus intensity shifts the firing profile from tonic to phasic firing [7], consistent with the model's prediction. The model also suggests that the onset-offset responses can be replicated with large p_E and p_I (≈ 1) and small changes in the delay of inhibition (Fig. 6). This offers an alternative mechanism to those previously proposed, which involve biophysical properties of neurons (Koppp-Scheinpfulug 2011, Hancock and Voigt, 1999), or network level dynamics (Bondanelli et al., 2021). In cortex, there is strong evidence that the onset and/or offset responses are inherited from upstream subcortical regions [40, 23], though there is evidence from experiments [20] and theory [22]that they may also arise *de novo* within cortex. Moreover, the presence of tonically responding neurons indicate the presence of sustained excitatory inputs, which together with tonically active inhibitory neurons, are prerequisite for the mechanism proposed by the model.

If incoming afferents are topographically-organized, then the spatiotemporal profiles shown in Fig. 7 is equivalent to the receptive field of a neuron at the center of the network. That is, the response of a single neuron to a range of stimuli (tuning curve) is equivalent to the response of a group of adjacent neurons to a single stimulus. Interpreted in this way, the model predicts that the firing response of a neuron will change both quantitatively and qualitatively, depending on the magnitude of the stimulus and how closely it matches the neuron's optimal stimulus. Such changes in response properties with stimulus parameter has been observed experimentally [40].

Limitations

The theory is based on three key assumptions. The first is that calculation of p_{net} assumes inhibitory inputs sum linearly with and "cancel" out excitatory inputs . However, synaptic inputs could sum sublinearly under physiological conditions because conductances can lead to shunting by inhibition. Although this issue was alleviated by including a term that accounts for conductances changes (eq. 5), the relative locations of the E and I contacts on the different compartments of the neuron must be considered when deciding to include the correction term. Moreover, the model does not account for heterogeneity in the size of the EPSPs and IPSPs. To simplify analyses, the size of the IPSPs were all expressed as a fraction (k_a) of the EPSPs. In reality, the size of the PSPs depend on several factors including location on the dendritic tree or receptor properties.

A second assumption is that the constants (k_n, k_a, k_q, k_r) that multiply p_I are chosen such that the product falls between 0 and 1, which is necessary for interpreting p_I as a probability. In the transient regime, this condition is likely satisfied under biological conditions because $k_n \approx 0.15-0.20$ [30, 31] and the IPSP amplitudes are comparable to EPSP amplitudes [1, 32, 2]. However, for

sustained stimuli, it less clear that the condition holds because the firing rate of some inhibitory cells (e.g. fast spiking cells) can be quite high, which may cause p_I to exceed 1. In practice, this can be addressed by capping $k_n k_q k_r p_I$ to 1, which should have minimal impact on firing rate calculations, as the firing rate rate is zero if the product is greater than or equal to 1.

The final assumption is that the recurrent connections do not contribute significantly to the evoked firing rate. For brief stimuli, recurrent activity is likely to have a smaller impact on firing ([33], but see [41, 42]). In cortex, the connection probability between E neurons is relatively low [2, 34] meaning that if the active area is confined to a small region (as may be the case for topographically-organized afferents), the small number of local E neurons that are recruited would not contribute significanlty to firing, as suggested by simulations [33]. However, this assumption may not hold for longer stimuli, where sustained excitatory drive could be enough to activate neighboring neurons.

Future directions

A simple model based on a feedforward inhibitory circuit has been developed, successfully capturing many key stimulus-evoked responses and input-output properties. However, it will be important to expand the model to incorporate recurrently connected networks and to develop formal mathematical analyses [43] that can offer guidelines for applying the model to wide range of circuit configurations observed in the nervous system.

References

[1] Anne-Marie M Oswald and Reyes. "Maturation of intrinsic and synaptic properties of layer 2/3 pyramidal neurons in mouse auditory cortex". In: *Journal of neurophysiology* 99.6 (2008), pp. 2998–3008.

[2] Robert B Levy and Reyes. "Spatial profile of excitatory and inhibitory synaptic connectivity in mouse primary auditory cortex". In: *Journal of Neuroscience* 32.16 (2012), pp. 5609–5619.

[3] Frances S Chance, Larry F Abbott, and Alex D Reyes. "Gain modulation from background synaptic input". In: *Neuron* 35.4 (2002), pp. 773–782.

[4] Matteo Carandini. "Amplification of trial-to-trial response variability by neurons in visual cortex". In: *PLoS biology* 2.9 (2004), e264.

[5] Ian M Finn, Nicholas J Priebe, and David Ferster. "The emergence of contrast-invariant orientation tuning in simple cells of cat visual cortex". In: *Neuron* 54.1 (2007), pp. 137–152.

[6] DP Phillips and DR Irvine. "Responses of single neurons in physiologically defined primary auditory cortex (AI) of the cat: frequency tuning and responses to intensity." In: *Journal of neurophysiology* 45.1 (1981), pp. 48–58.

[7] Benedikt Grothe. "Interaction of excitation and inhibition in processing of pure tone and amplitude-modulated stimuli in the medial superior olive of the mustached bat". In: *Journal of Neurophysiology* 71.2 (1994), pp. 706–721.

[8] Wensheng Sun et al. "Decoding sound level in the marmoset primary auditory cortex". In: *Journal of neurophysiology* 118.4 (2017), pp. 2024–2033.

[9] David M Schneider, Janani Sundararajan, and Richard Mooney. "A cortical filter that learns to suppress the acoustic consequences of movement". In: *Nature* 561.7723 (2018), pp. 391–395.

[10] Carrie J McAdams and John HR Maunsell. "Effects of attention on orientation-tuning functions of single neurons in macaque cortical area V4". In: *Journal of Neuroscience* 19.1 (1999), pp. 431–441.

[11] Carrie J McAdams and R Clay Reid. "Attention modulates the responses of simple cells in monkey primary visual cortex". In: *Journal of Neuroscience* 25.47 (2005), pp. 11023–11033.

[12] Kenneth D Harris and Alexander Thiele. "Cortical state and attention". In: *Nature reviews neuroscience* 12.9 (2011), pp. 509–523.

[13] Katie A Ferguson and Jessica A Cardin. "Mechanisms underlying gain modulation in the cortex". In: *Nature Reviews Neuroscience* 21.2 (2020), pp. 80–92.

[14] Bryan A Seybold et al. "Inhibitory actions unified by network integration". In: *Neuron* 87.6 (2015), pp. 1181–1192.

[15] Tina Gothner et al. "Sustained activation of PV+ interneurons in core auditory cortex enables robust divisive gain control for complex and naturalistic stimuli". In: *Cerebral Cortex* 31.5 (2021), pp. 2364–2381.

[16] David J Heeger. "Normalization of cell responses in cat striate cortex". In: *Visual neuroscience* 9.2 (1992), pp. 181–197.

[17] Matteo Carandini and David J Heeger. "Summation and division by neurons in primate visual cortex". In: *Science* 264.5163 (1994), pp. 1333–1336.

[18] IO Volkov and AV Galazjuk. "Formation of spike response to sound tones in cat auditory cortex neurons: interaction of excitatory and inhibitory effects". In: *Neuroscience* 43.2-3 (1991), pp. 307–321.

[19] Gregg H Recanzone. "Response profiles of auditory cortical neurons to tones and noise in behaving macaque monkeys". In: *Hearing research* 150.1-2 (2000), pp. 104–118.

[20] Magdalena Solyga and Tania Rinaldi Barkat. "Emergence and function of cortical offset responses in sound termination detection". In: *Elife* 10 (2021), e72240.

[21] Bettina Joachimsthaler et al. "Quantitative analysis of neuronal response properties in primary and higher-order auditory cortical fields of awake house mice (M us musculus)". In: *European Journal of Neuroscience* 39.6 (2014), pp. 904–918.

[22] Giulio Bondanelli et al. "Network dynamics underlying OFF responses in the auditory cortex". In: *Elife* 10 (2021), e53151.

[23] Ben Scholl, Xiang Gao, and Michael Wehr. "Nonoverlapping sets of synapses drive on responses and off responses in auditory cortex". In: *Neuron* 65.3 (2010), pp. 412–421.

[24] Conny Kopp-Scheinpflug, James L Sinclair, and Jennifer F Linden. "When sound stops: offset responses in the auditory system". In: *Trends in neurosciences* 41.10 (2018), pp. 712–728.

[25] Michael Wehr and Anthony M Zador. "Balanced inhibition underlies tuning and sharpens spike timing in auditory cortex". In: *Nature* 426.6965 (2003), pp. 442–446.

[26] AYY Tan and M Wehr. "Balanced tone-evoked synaptic excitation and inhibition in mouse auditory cortex". In: *Neuroscience* 163.4 (2009), pp. 1302–1315.

[27] Judith A Hirsch et al. "Synaptic integration in striate cortical simple cells". In: *Journal of neuroscience* 18.22 (1998), pp. 9517–9528.

[28] Jaime De La Rocha et al. "Linking the response properties of cells in auditory cortex with network architecture: cotuning versus lateral inhibition". In: *Journal of Neuroscience* 28.37 (2008), pp. 9151–9163.

[29] Max L Schiff and Reyes. "Characterization of thalamocortical responses of regular-spiking and fast-spiking neurons of the mouse auditory cortex in vitro and in silico". In: *Journal of neurophysiology* 107.5 (2012), pp. 1476–1488.

[30] Daniel Maxim Iascone et al. "Whole-neuron synaptic mapping reveals spatially precise excitatory/inhibitory balance limiting dendritic and somatic spiking". In: *Neuron* 106.4 (2020), pp. 566–578.

[31] Clermont Beaulieu. "Numerical data on neocortical neurons in adult rat, with special reference to the GABA population". In: *Brain research* 609.1-2 (1993), pp. 284–292.

[32] Anne-Marie M Oswald and Reyes. "Development of inhibitory timescales in auditory cortex". In: *Cerebral Cortex* 21.6 (2011), pp. 1351–1361.

[33] Robert B Levy and Reyes. "Coexistence of lateral and co-tuned inhibitory configurations in cortical networks". In: *PLoS computational biology* 7.10 (2011), e1002161.

[34] Luke Campagnola et al. "Local connectivity and synaptic dynamics in mouse and human neocortex". In: *Science* 375.6585 (2022), eabj5861.

[35] John H Maunsell and Jay R Gibson. "Visual response latencies in striate cortex of the macaque monkey". In: *journal of Neurophysiology* 68.4 (1992), pp. 1332–1344.

[36] Hugh R Wilson and Jack D Cowan. "Excitatory and inhibitory interactions in localized populations of model neurons". In: *Biophysical journal* 12.1 (1972), pp. 1–24.

[37] Daniel B Rubin, Stephen D Van Hooser, and Kenneth D Miller. "The stabilized supralinear network: a unifying circuit motif underlying multi-input integration in sensory cortex". In: *Neuron* 85.2 (2015), pp. 402–417.

[38] Andrew YY Tan et al. "Unbalanced synaptic inhibition can create intensity-tuned auditory cortex neurons". In: *Neuroscience* 146.1 (2007), pp. 449–462.

[39] Ling Qin et al. "Neural and behavioral discrimination of sound duration by cats". In: *Journal of Neuroscience* 29.50 (2009), pp. 15650–15659.

[40] Ling Qin et al. "Comparison between offset and onset responses of primary auditory cortex ON–OFF neurons in awake cats". In: *Journal of neurophysiology* 97.5 (2007), pp. 3421–3431.

[41] Ehud Ahissar, Ronen Sosnik, and Sebastian Haidarliu. "Transformation from temporal to rate coding in a somatosensory thalamocortical pathway". In: *Nature* 406.6793 (2000), pp. 302–306.

[42] Jeremie Barral, Wang, and Reyes. "Propagation of temporal and rate signals in cultured multilayer networks". In: *Nature communications* 10.1 (2019), pp. 1–14.

[43] Alex D Reyes. "Mathematical framework for place coding in the auditory system". In: *PLoS computational biology* 17.8 (2021), e1009251.

Appendix

Simulation parameters

Simulations were performed with a custom program written in the Matlab environment. The network consisted a reference neuron and 50-250 local inhibitory neuron. Both cell types received 100-250 afferent from an excitatory source, with the reference cells also receiving inhibitory inputs from the local interneurons.

Neurons were leaky-integrate-and-fire (LIF) neuron with : resistance = 75MΩ, resting potential = -70 mV, membrane time constant = 10 ms, action potential threshold = -55mV. The unitary synaptic current followed an alpha function ($\mu = (t/\tau).*exp(1-t/\tau), \tau = 2ms;$). For current clamp, μ was scaled by 0.0103 nA, and -0.0103 nA, which produced EPSPs and IPSP with amplitudes of 250 µV and -250 µV, respectively. For conductance clamp, μ was scaled by $g_E(v - V_{exc})$ where $g_E = 0.147nS, V_E = 0$ mV for E synapses and by $g_I(v - V_I)$ where $g_I = 1.045nS, V_I = -80$ mV for inhibitory synapses. Synaptic barrages were generated by convolving the unitary synaptic current or conductance with a Poisson train of a specified rate.

Calculating firing probability with transient input

Relating probabilities to cellular and network properties

The following refers to a reference neuron that receives n_E excitatory inputs from an external source and n_I inhibitory inputs from local inhibitory interneurons, with $n_I \leq n_E$ and for the moment, no delay in the arrival of EPSPs and IPSPs. The EPSPs and IPSPs evoked from the external afferents and inhibitory interneurons, respectively, are small. In the presence of a stimulus, the EPSPs from the afferents appear in the reference cell and in the local interneurons with probability p_E . The interneurons will fire with probability of p_I , either as a result of the external stimulus and/or some background activity.

In the presence of the stimulus, an average of $n_E p_E$ excitatory inputs appear in the reference cell. Of the $n_I p_I$ inhibitory inputs that arrive in the reference cell, $p_E n_I p_I$ will arrive at the same time as the excitatory inputs. Thus, the net number of excitatory inputs is $n_{net} = n_E p_E - p_E n_I p_I$. If the amplitude (in mV) of the EPSP is a_E and that of the IPSP is a_I, the average amplitude of the combined PSPs is:

$$\begin{aligned} a_{net} &= n_E p_E a_E - p_E n_I p_I a_I \\ &= n_E p_E a_E - p_E k_n n_E p_I k_a a_E \\ &= n_E a_E p_E (1 - k_n k_a p_I) \\ &= n_E a_E p_E (1 - \hat{p}_I) \\ &= n_E a_E p_{net} \end{aligned} \tag{1}$$

The probability of evoking an action potential is the probability that a_{net} exceeds threshold for firing v_θ or, equivalently, the probability that the net number of EPSPs exceed the minimum threshold number ($n_\theta = \frac{v_\theta}{a_{net}}$). The firing probability is then calculated from the cumulative binomial distribution (β):

$$p_f = prob(n_{net} \geq n_\theta) = 1 - \beta(n_E, n_\theta, p_{net}) \tag{2}$$
$$\beta = \sum_{i=0}^{n_\theta} \binom{n_E}{i} p_{net}(t)^i (1 - p_{net}(t))^{n_E - i}$$

The next step is to derive a more general form that relaxes the assumption that the E and I inputs arrive simultaneously. A brief stimulus evokes a composite EPSP ($C_E(t)$, the sum of several unitary EPSPs) and the accompanying composite IPSP ($C_I(t)$). The composite PSPs is composed of unitary PSPs so that the average composite is given by:

$$\begin{aligned} C_E(t) &= a_E n_E p_E \mu(t) \\ C_I(t) &= a_I n_I p_I \mu(t) \\ &= -k_a k_n a_E n_E p_I \mu(t) \\ &= -a_E n_E (k_a k_p p_I) \mu(t), 0 \leq k_a k_p p_I \leq 1 \end{aligned} \tag{3}$$

where p is the probability that the unitary PSP appears, a (in mV) is the amplitude of the PSP, n is the number of inputs, and $u(t)$ is the time course of the PSP (alpha function) with peak amplitude of 1. The summed composite, with inhibition conditioned on appearing at same time as the EPSP, is then:

$$\begin{aligned} C_{tot}(t) &= a_E n_E p_E \mu(t) - p_E a_E n_E (k_a k_p p_I) \mu(t) \\ &= a_E n_E \mu(t)(p_E - p_E(k_a k_p p_I)) \\ &= a_E n_E \mu(t) p_E (1 - k_a k_p p_I) \\ &= a_E n_E \mu(t) p_{net} \end{aligned}$$

If p is distributed over time, as would occur if the EPSPs arrival are jittered, the composites are obtained by the convolutions:

$$\begin{aligned} C_E(t) &= a_E n_E \int p_E \mathcal{N}(\mu_t, \sigma_t^2) * u(t - \tau) d\tau \\ &= a_E n_E \hat{p}_E(t) \\ C_I(t) &= a_I n_I \int p_I(t) * u(t - \tau) d\tau \\ &= -k_a a_E k_n n_E \int p_I(t) * u(t - \tau) d\tau; 0 \leq k_a k_n \leq 1 \\ &= -a_E n_E k_a k_n \hat{p}_I(t) \end{aligned} \tag{4}$$

$$\tag{5}$$

where $\mathcal{N}(\mu_t, \sigma_t^2)$ is a normal distribution, k_n is the ratio of n_E to the number of inhibitory inputs n_I, and k_a is the ratio of unitary IPSP amplitude to unitary EPSP amplitude. The summed composite, with the inhibitory component conditioned on being coincident with the excitation, is then:

$$\begin{aligned} C_{tot}(t) &= \hat{p}_E(t) a_E n_E p_E - \hat{p}_E(t) \hat{p}_I(t) a_E n_E k_a k_n \\ &= a_E n_E (\hat{p}_E(t) - \hat{p}_E(t) \hat{p}_I(t) k_a k_n) \\ &= a_E n_E (\hat{p}_E(t)(1 - k_a k_n \hat{p}_I(t)) \end{aligned}$$

The time-varying probabilities can be estimated from $C_E(t)$ and $C_I(t)$ obtained with the simulations:

$$\hat{p}_E(t) = \frac{C_E(t)}{a_E n_E} \tag{6}$$
$$k_a k_n \hat{p}_I(t) = \frac{C_I(t)}{-a_E n_E}$$

The probability that the cell will fire is equal to the probability that the voltage at a given time exceeds the action potential threshold v_θ. Assuming that the membrane potential distribution at a given time is normal with mean $\mu = n_E k_a a_E p_{net}$ and standard deviation $\sigma = \sqrt{(}n_E k_a a_E p_{net}(1 - p_{net}))$, the probability that the composite EPSP exceeds threshold is given by:

$$prob(v \geq v_\theta) = (1 - \Phi(v_\theta, \mu, \sigma)) \tag{7}$$

where Φ is the normal cumulative distribution function (green curve in Fig. 2, bottom of main text).

Finally, the probability that the action potential will occur at a specific time t_i is equal to the probability of firing at time t_i $(= p_f(t_i))$ multiplied by the probability that it didn't occur at earlier times $(p_f(t_{i-1})p_f(t_{i-2}), \dots)$.

$$prob(\text{spike at } t_i) = p_f(t_i)\pi_{j=1}^{i-1}(1 - p_f(t_j)) \tag{8}$$

This is the magenta curve in Fig.2, middle traces.

Calculating firing probability with sustained input

Many neurons, in response to sustained synaptic input, enter the oscillatory firing regime. Typically, the firing rate depends on the mean synaptic current (so-called firing rate-current, or f-I curve). During a sustained stimulus, the afferents and I neurons trains of EPSPs and IPSPs, respectively, producing a synaptic barrage in the postsynaptic neuron (black).

The average excitatory current from the external afferents is given by:

$$i_E(t) = p_E(t) n_E q_E r_E \tag{9}$$

Similarly, the average inhibitory current, conditioned on the afferent input appearing at the same time (eq. 1), is given by:

$$i_I(t) = -p_E(t) p_I(t) n_I q_I r_I \tag{10}$$

Assuming for now that the currents add linearly (relaxed below), the net current is:

$$\begin{aligned} i_{net}(t) &= i_E(t) + i_I(t) \\ &= p_E(t) n_E q_E r_E - p_E(t) p_I(t) n_I q_I r_I \\ &= p_E(t) n_E q_E r_E - p_E(t) p_I(t) k_n n_E k_q q_E k_r r_E \\ &= n_E q_E r_E p_E(t)(1 - k_n k_q k_r p_I(t)) \end{aligned} \tag{11}$$

where $k_n = \frac{n_I}{n_E}$ is the ratio of number of inhibitory inputs to excitatory inputs, $k_q = \frac{q_I}{q_E}$ is the ratio of the inhibitory and excitatory charges and $k_r = \frac{r_I}{r_E}$ is the ratio of inhibitory rate to external input rate.

The evoked firing rate in the oscillatory regime is then calculated by:

$$r_{osc}(t) = S(i_{net}(t)) \tag{12}$$

where S is an input-output function (e.g. experimentally measured f-I curve), a model neuron, or in the case of an LIF neuron as $1000/(-\tau_m * ln(1-(i_{rh}/i_{net})))$ where i_{rh} is the rheobase or minimum current needed to evoke firing.

In the sub-oscillatory regime, spurious firing occurs because of variability that causes the synaptic current i_{syn} to exceed rheobase. This probability is given by:

$$prob(i_{syn}(t) \geq i_{rh}) = (1 - \beta(n_E, n_\theta, p_{net}(t))) \tag{13}$$

where β is the binomial cumulative distribution function:

$$\beta(n_E, n_\theta, p_{net}) = \sum_{i=0}^{n_\theta} \binom{n_E}{i} p_{net}^i (1 - p_{net})^{n_E - i} \tag{14}$$

This function saturates to 1 at close to the start of the oscillatory regime. Scaling the function by the minimum evoked firing in the oscillatory regime joins the curves at the two regimes. The firing rate is defined to be the larger of the two:

$$\begin{aligned} r_{fluct} &= r_{rh}(1 - \beta(n_E, n_\theta, p_{net})) \\ r_f &= max(r_{fluct}, r_{osc}) \end{aligned} \tag{15}$$

.

Correcting for conductance

The voltage-dependent unitary postsynaptic current for E and I are, respectively, $\mu_E(v,t) = g_E(t)(v - V_{exc})$ and $\mu_I(v,t) = g_I(t)(v - V_{inh})$, where the g's are conductances and the V's are the equilibrium potentials. The voltage-dependent charges are therefore:

$$\begin{aligned} q_E(v) &= (v - V_{exc}) \int g_E(t)dt \ (\frac{coul}{V - sec}) \\ &= G_E(v - V_{exc}) \\ q_I(v) &= (v - V_{inh}) \int g_I(t)dt \\ &= G_I(v - V_{inh}) \end{aligned} \tag{16}$$

The voltage-dependent synaptic current barrages are then given by:

$$
\begin{aligned}
i_E(v) &= p_E r_E n_E G_E(v - V_{exc}) \\
i_I(v) &= p_E p_I r_I n_E G_I(v - V_{inh}) \\
i_{net}(v) &= p_E r_E n_E G_E(v - V_{exc}) + p_E p_I r_I n_I G_I(v - V_{inh}) \\
&= p_E r_E n_E G_E(v - V_{exc}) + p_E p_I k_r r_E k_n n_E k_g G_E(v - V_{inh}) \\
&= r_E n_E G_E(p_E(v - V_{exc}) + p_E p_I k_r k_n k_g(v - V_{inh})) \\
&= r_E n_E G_E(p_E(v - V_{exc}) + p_E p_I k_r k_n k_g(\frac{v - V_{inh}}{v - V_{exc}})(v - V_{exc}) \\
&= r_E n_E G_E(p_E(v - V_{exc}) - p_E p_I k_r k_n k_g(-(\frac{v - V_{inh}}{v - V_{exc}}))(v - V_{exc}) \\
&= r_E n_E G_E(p_E(v - V_{exc}) - p_E p_I k_r k_n k_g k_v(v - V_{exc})) \\
&= r_E n_E G_E(v - V_{exc})(p_E - p_E p_I k_r k_n k_g k_v) \\
&= r_E n_E G_E(v - V_{exc}) p_{net}
\end{aligned}
\tag{17}
$$

where k_g is the ratio $\frac{g_I}{g_E}$ and $k_v = -(\frac{v - V_{inh}}{v - V_{exc}}); v_{inh} \leq v \leq v_{inh}/(1 + k_r k_n k_g))$;